Chemical Science

ROYAL SOCIETY OF CHEMISTRY

EDGE ARTICLE

View Article Online
View Journal | View Issue

Cite this: *Chem. Sci.*, 2023, **14**, 8624

All publication charges for this article have been paid for by the Royal Society of Chemistry

A π-conjugated covalent organic framework enables interlocked nickel/photoredox catalysis for light-harvesting cross-coupling reactions†

Ayan Jati, Suranjana Dam,‡ Shekhar Kumar,‡ Kundan Kumar‡ and Biplab Maji *

Received 12th May 2023
Accepted 18th July 2023

DOI: 10.1039/d3sc02440g

rsc.li/chemical-science

Covalent organic frameworks (COFs) are an outstanding platform for heterogeneous photocatalysis. Herein, we synthesized a pyrene-based two-dimensional C=C linked π-conjugated COF *via* Knoevenagel condensation and anchored Ni(II)-centers through bipyridine moieties. Instead of traditional dual metallaphotoredox catalysis, the mono-metal decorated Ni@Bpy-sp^{2}c-COF interlocked the catalysis mediated by light and the transition metal. Under light irradiation, enhanced energy and electron transfer in the COF backbone, as delineated by the photoluminescence, electrochemical, and control experiments, expedited the excitation of Ni centers to efficiently catalyze diverse photocatalytic C–X (X = B, C, N, O, P, S) cross-coupling reactions with efficiencies orders of magnitude higher than the homogeneous controls. The COF catalyst tolerated a diverse range of coupling partners with various steric and electronic properties, delivering the products with up to 99% yields. Some reactions were performed on a gram scale and were applied to diversify pharmaceuticals and complex molecules to demonstrate the synthetic utility.

Introduction

Over recent years, developments in covalent organic frameworks (COFs) have led to significant attention in heterogeneous catalysis.[1] The controllable engineering of these porous crystalline platforms provides the required stability and offers enough flexibility to incorporate active catalytic sites with subtle control of catalytic functions.[2] In particular, the inherent light harvesting and energy transfer capabilities of COFs due to their π-extended in-plane structure could be tuned by pre or post-decoration.[3] However, the field of COF-based photocatalysis is mainly dominated by solar energy sequestering proton and carbon dioxide reduction reactions,[4] even though COFs could be envisaged as a suitable platform to anchor a redox-active precatalyst and to be used as a sustainable sensitizer in light-mediated fine chemical synthesis.[5]

Photocatalysis creates a sustainable alternative to harsh thermal conditions in chemical bond activation and bond-forming reactions.[6] Recently, strategies employing nickel precursors combined with visible-light photocatalysis *via* photoredox, energy transfer, and charge transfer were used for forging carbon–carbon and carbon–heteroatom bonds.[7] The merger of the excited-state photochemistry of sensitizers with nickel-mediated substrate activation and electronic structure modification *via* electron and energy transfer expands opportunities without needing stoichiometric redox equivalents and high-energy ultraviolet light.[8] Compared to the typically known precious metal-derived homogeneous photocatalysts, heterogeneous photocatalysts open a sustainable avenue.[9] In particular, placing the photoactive and redox catalytic units in proximity enhances their photoredox communication compared to their Brownian motion-limited homogeneous and semi-heterogeneous counterparts.[5b,10] In this regard, recently, we showed that the COF pores could be post-synthetically engineered to incorporate nickel and photosensitizing iridium centers in proximity that allowed visible light-induced C–N cross-coupling in high yields maintaining high robustness and reusability.[11] Herein, we report the successful installation of a single redox center instead of dual metals into COF pores where the synchronized participation of the COF backbone as a photocatalyst achieved diverse visible light-driven cross-coupling reactions (Fig. 1).

We selected a pyrene-based sp^2 carbon-conjugated COF as a potential photocatalyst for its excellent chemical stability and photoluminescence properties.[4b,f,12] The Bpy-sp^{2}c-COF was synthesized *via* the Knoevenagel condensation reaction, and the nickel(II) chloride center was installed through bipyridine moieties (Fig. 1a). Notably, the singular Ni@Bpy-sp^{2}c-COF catalyzed eight visible light-mediated C–X (X = B, C, N, O, P, S) bond-forming cross-coupling reactions (Fig. 1b).[8a,13] We proposed that the synergistic participation of the light-harvesting COF backbone and the redox-active Ni-unit interlocks the catalytic cycles

Department of Chemical Sciences, Indian Institute of Science Education and Research Kolkata, Mohanpur 741246, WB, India. E-mail: bm@iiserkol.ac.in

† Electronic supplementary information (ESI) available. CCDC 2216257, 2216734, 2216735 and 2216737. For ESI and crystallographic data in CIF or other electronic format see DOI: https://doi.org/10.1039/d3sc02440g

‡ These authors contributed equally.

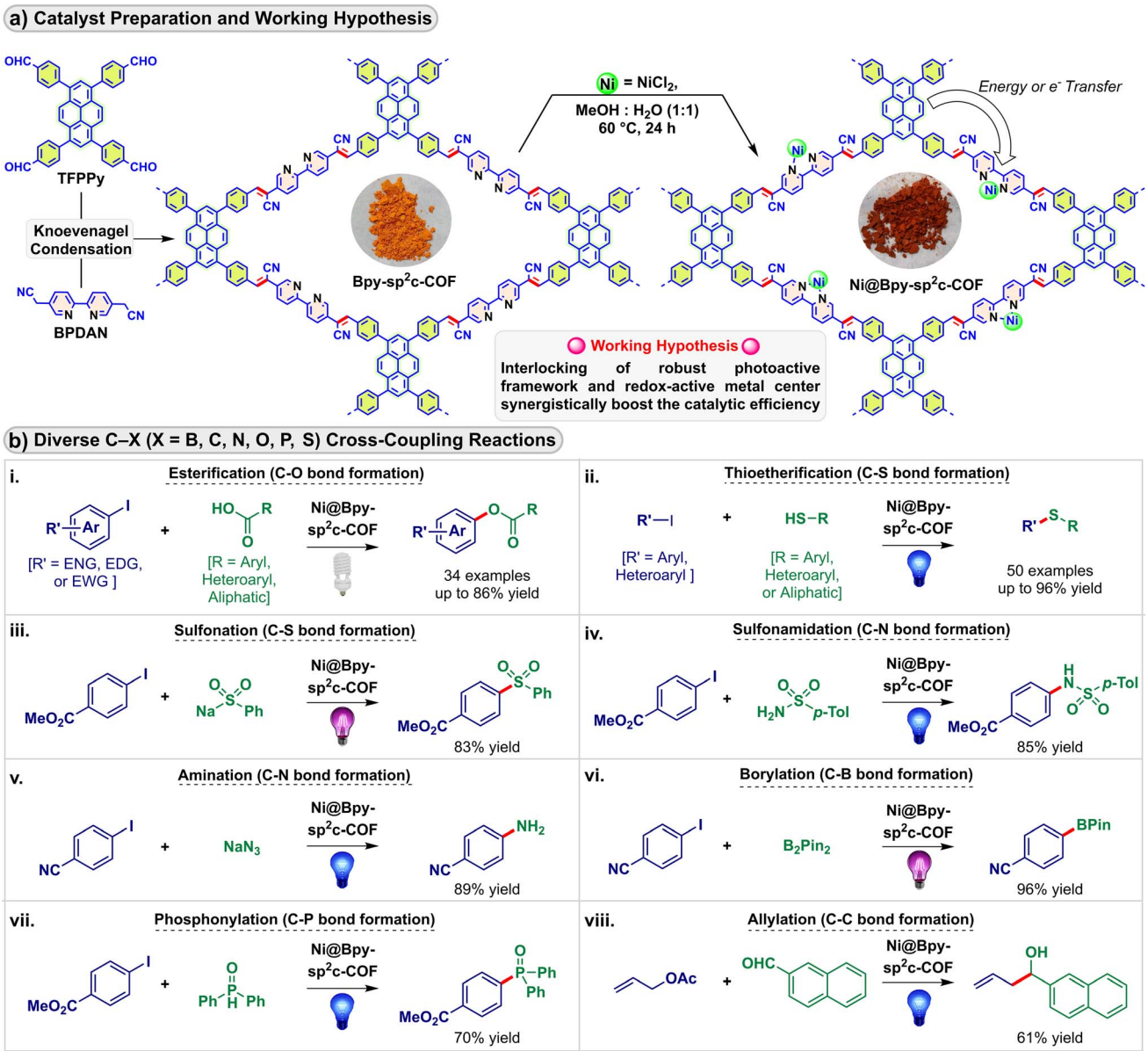

Fig. 1 (a) Catalyst preparation *via* $NiCl_2$ installation in the Bpy-sp^{2}c-COF and the working hypothesis; and (b) application of the Ni@Bpy-sp^{2}c-COF catalyst in different C–X (X = B, C, N, O, P, S) cross-coupling reactions with isolated yields of the products. ENG = electron neutral group, EDG = electron donating group, EWG = electron withdrawing group.

mediated by light and the transition metal and facilitates the dual catalysis with efficiency orders of magnitude higher than its homogeneous counterpart.[14] Besides, the anchored COF backbone prevented the nickel-black formation and leaching, enabling selective coupling of the reactants with diverse steric and electronic properties, maintaining high catalytic efficiency (high turnover number and frequency), and reusability. A few of these reactions can be performed on a gram scale and can diversify bioactive and drug molecules.

Results and discussion

Bpy-sp^{2}c-COF was synthesized *via* the condensation of 1,3,6,8-tetrakis(4-formylphenyl)pyrene (TFPPy) and 5,5′-diacetonitrile-2,2′-bipyridine (BPDAN) under the solvothermal procedure following a modified procedure previously reported by Cooper (Fig. 1a, S1†).[4b] We have found a longer reaction time, and washing with *N*,*N*-dimethyl acetamide is beneficial for a higher surface area, *vide infra*. The highly conjugated framework provides an excellent platform for photosensitization with a functional bipyridine linker toward post-synthetic engineering. The crystalline ordered structure of Bpy-sp^{2}c-COF was further confirmed by the powder X-ray diffraction (PXRD) analysis that showed a peak at 3.2° (2θ), corresponding to the reflection from the (110) plane (Fig. S2†).[5c]

Bpy-sp^{2}c-COF was treated with $NiCl_2$ in H_2O/MeOH at 60 °C to form Ni@Bpy-sp^{2}c-COF with random Ni-sites in the framework. The insertion of Ni(II) centers in Bpy-sp^{2}c-COF was corroborated

by comparing pristine COF and Ni@Bpy-sp^{2}c-COF. Infrared (IR) spectroscopy analysis of Bpy-sp^{2}c-COF divulged a red-shift of the C≡N stretching frequency (at 2216 cm^{-1}) compared to BPDAN (at 2256 cm^{-1}) (Fig. 2a, S3†). This red shift supported the COF backbone formation, where the cyano groups participated in extended π-conjugation in the framework *via* the construction of the C=C bond.[4b,12a] The aldehydic C–H stretching frequencies 2810 cm^{-1} and 2720 cm^{-1} are almost absent in the COF, and a weak peak suggests the presence of residual aldehyde groups at the edge of the backbone. The IR spectrum of Ni@Bpy-sp^{2}c-COF showed no perceptible change compared to Bpy-sp^{2}c-COF, revealing the retention of the backbone during the post-metalation of Bpy-sp^{2}c-COF.

The Brunauer–Emmett–Teller (BET) surface areas calculated for the Bpy-sp^{2}c-COF and Ni@Bpy-sp^{2}c-COF are 610 and 268 m^2 g^{-1}, respectively (Fig. 2b). The total pore volumes are calculated as 0.456, and 0.176 cc g^{-1}, respectively. A decrease in BET surface area observed for the Ni@Bpy-sp^{2}c-COF could rationalize the $NiCl_2$ incorporation in the Bpy-sp^{2}c-COF backbone.

Transmission electron microscopy (TEM) and scanning electron microscopy (SEM) images confirmed that the micro rods and cluster shapes are present in Ni@Bpy-sp^{2}c-COF (Fig. 2c). Furthermore, the images suggested the absence of metal oxides or nanoparticles during the insertion of $NiCl_2$ in the COF backbone (Fig. S4 and S6†). In addition, energy-dispersive X-ray (EDX) mapping using TEM and SEM images

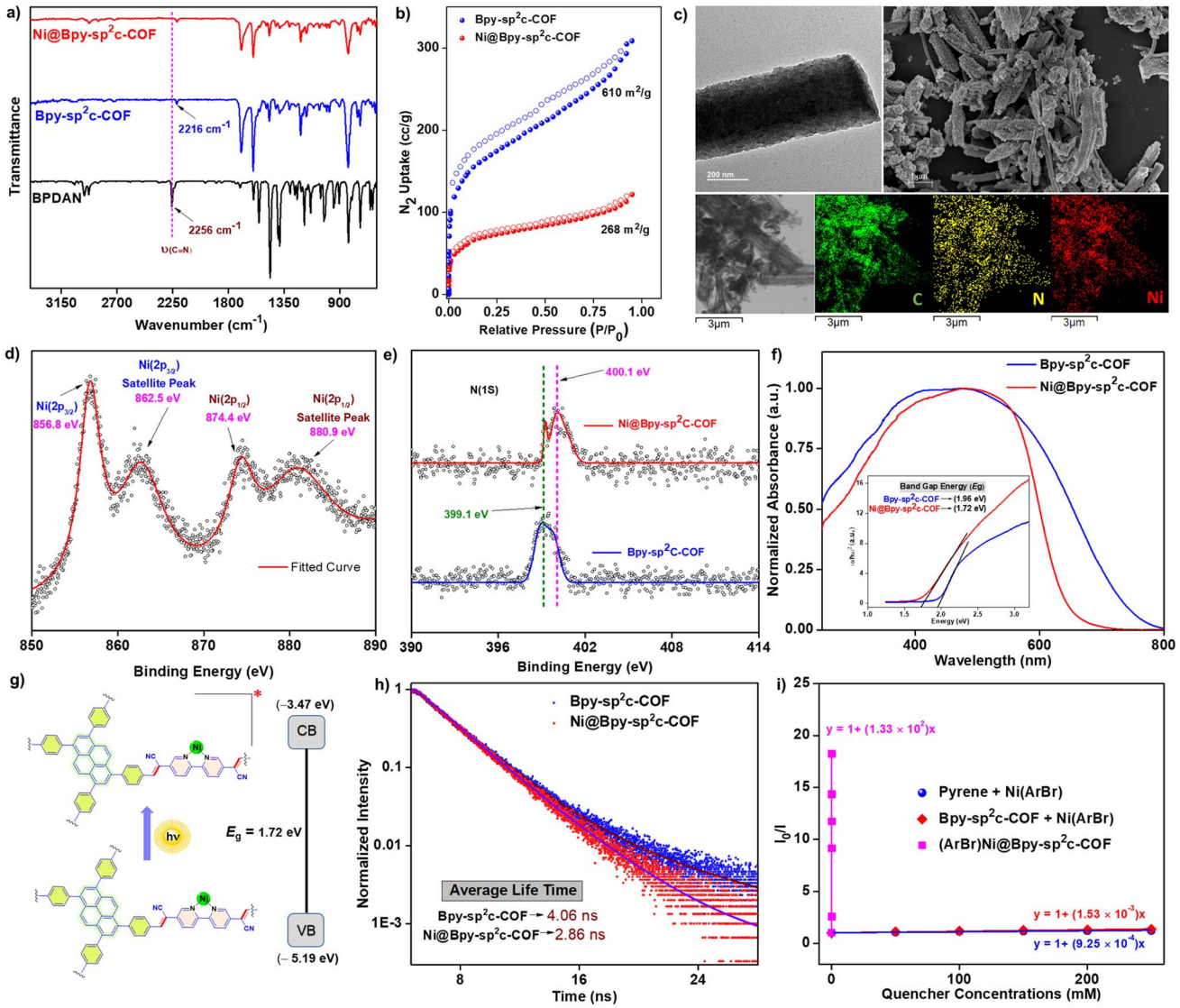

Fig. 2 (a) IR analysis of BPDAN, Bpy-sp^{2}c-COF, and Ni@Bpy-sp^{2}c-COF; (b) BET surface analysis of Bpy-sp^{2}c-COF before and after Ni metal insertion; (c) TEM image (top left corner), SEM image (top right corner), elemental mapping (below) of Ni@Bpy-sp^{2}c-COF; (d) Ni(2p) XPS analysis of Ni@Bpy-sp^{2}c-COF (850 eV to 890 eV region); (e) comparative N(1s) XPS analysis of Bpy-sp^{2}c-COF and Ni@Bpy-sp^{2}c-COF (390 eV to 414 eV region); (f) comparative UV-reflectance spectra and Tauc plot (inset) of Bpy-sp^{2}c-COF and Ni@Bpy-sp^{2}c-COF; (g) the light absorbing ability of Ni@Bpy-sp^{2}c-COF and arrangements of the valence band (VB) and conduction band (CB); (h) average lifetime from time-correlated single-photon counting (TCSPC) experiments; (i) comparative Stern–Volmer photoluminescence quenching for pyrene and Bpy-sp^{2}c-COF by the Ni(ArBr) complex (Ar = 4-CNC$_6$H$_4$), and different Ni-loaded Ni(ArBr)@Bpy-sp^{2}c-COF.

showed that the Ni metal is evenly distributed in the Ni@Bpy-sp^{2}c-COF matrix (Fig. 2c, S5 and S7†). Nevertheless, the comparative analysis of images revealed the unaltered overall morphology before and after the decoration of Bpy-sp^{2}c-COF. The X-ray photoelectron spectroscopy (XPS) spectra of Ni@Bpy-sp^{2}c-COF exhibited two distinct peaks at 856.8 eV and 874.4 eV corresponding to Ni($2p_{3/2}$) and Ni($2p_{1/2}$) of Ni(II), respectively (Fig. 2d). Additionally, satellite peaks appeared at 862.5 eV and 880.9 eV without metallic Ni and NiO impurities. The relative analysis of N(1s) XPS spectra for Bpy-sp^{2}c-COF and Ni@Bpy-sp^{2}c-COF demonstrated a slight shift in the N(1s) mean binding energy peak from 399.1 eV to 400.1 eV (Fig. 2e). This result also supports the incorporation of the Ni(II) *via* bipyridine nitrogen centers. The XPS deconvoluted N (1s) spectra of Bpy-sp^{2}c-COF and Ni@Bpy-sp^{2}c-COF also showed the contribution of different nitrogen centers balanced with experimental data (Fig. S8†). Inductively coupled plasma-optical emission spectrometry (ICP-OES) analysis indicated that 2.65 wt% of Ni content was present in the Ni@Bpy-sp^{2}c-COF, which indicated that there was 0.45 mmol g^{-1} Ni in the overall COF. The thermogravimetric analysis (TGA) of Bpy-sp^{2}c-COF and Ni@Bpy-sp^{2}c-COF revealed excellent thermal stability (up to ~300 °C) even after decoration with $NiCl_2$ (Fig. S9†).

The UV-reflectance spectra of Ni@Bpy-sp^{2}c-COF displayed a broad absorption, specifically in the region 370 nm to 600 nm, suggesting the efficient visible-light absorption ability of this material (Fig. 2f). Furthermore, the band gap energies of Bpy-sp^{2}c-COF and Ni@Bpy-sp^{2}c-COF were calculated with the help of the Tauc plot (Fig. 2f-inset, detailed in Fig. S10†). The narrower band gap (1.72 eV) of Ni@Bpy-sp^{2}c-COF compared to Bpy-sp^{2}c-COF (1.96 eV) suggested that the insertion of the Ni(II)-center in the COF backbone enhanced the electron delocalization and lowered the gap. This bandgap energy is comparable to our previously reported Ni–Ir@TpBpy COF catalyst used for the photocatalytic C–N coupling reaction.[11] This also hints at the potential applicability of Ni@Bpy-sp^{2}c-COF in photocatalytic cross-coupling reactions.

The cyclic voltammetry (CV) experiments were performed for model compounds Ni(dtbbpy)Cl_2 and pyrene to model the feasibility of efficient electron transfer from the COF backbone to the Ni^{II}-center (Fig. S11a†). We have observed two reduction peaks at −1.67 V (R1), and −2.05 V (R2), *vs.* Ag/$AgNO_3$ corresponding to the $Ni^{II/I}$, and $Ni^{I/0}$ couples, respectively, for Ni(dtbbpy)Cl_2. The reduction peak for pyrene was observed at −2.65 V (R3). This indicated that the pyrene should efficiently reduce the Ni(II)-precatalyst to Ni(I)- or even Ni(0)-species for the subsequent oxidative addition with the aryl electrophiles. The CV of pristine Bpy-sp^{2}c-COF and metallated Bpy-sp^{2}c-COF was also performed to locate the conduction band (CB) energy from the reduction onset potential (Fig. S11b, Table S1†). The valence band (VB) position was estimated from the band gap (Fig. 2f and g). In addition, we have performed Mott–Schottky experiments. As shown in Fig. S12,† both the Bpy-sp^{2}c-COF and Ni@Bpy-sp^{2}c-COF showed positive slopes regardless of the varied frequencies. The flat band potentials for Bpy-sp^{2}c-COF and Ni@Bpy-sp^{2}c-COF were extrapolated as −0.90 V and −0.82 V *vs.* Ag/AgCl, respectively. The direct connection and interlocking between the Bpy-sp^{2}c-COF backbone with the Ni-center (distance near zero)[7d] and the VB/CB energy location with suitable band gap energy distribution triggered the photocatalytic catalytic efficiency (Fig. 2g).

The photoluminescence spectrum suggested that upon excitation by 390 nm light, the Ni@Bpy-sp^{2}c-COF emits at 460 nm (Fig. S13†). From the time-dependent emission spectrum, the excited state average lifetime of Ni@Bpy-sp^{2}c-COF was calculated to be 2.86 ns (Fig. 1h and S14†). In comparison, the lifetime of pristine Bpy-sp^{2}c-COF is 4.06 ns. The decreased lifetime from pristine COF to Ni@Bpy-sp^{2}c-COF clearly reinforces the efficient energy or electron transfer from the COF backbone to the Ni-center.

We then performed luminescence quenching studies to inspect the energy and electron transfer in Ni@Bpy-sp^{2}c-COF without an external electron donor. The complexes (ArBr)Ni(bpy) and (ArBr)Ni@Bpy-sp^{2}c-COF were synthesized using 4-bromobenzonitrile (Ar = 4-CNC_6H_4).[15] The luminescence of pyrene and Bpy-sp^{2}c-COF was efficiently quenched by the increasing concentration of (ArBr)Ni(bpy) in intermolecular experiments (Fig. 2i, detailed in Fig. S15†). Quenching constants $K_{sv} = 0.925\ M^{-1}$ (with pyrene) and $1.53\ M^{-1}$ (with Bpy-sp^{2}c-COF) were calculated by fitting the Stern–Volmer equation $(I_0/I) = 1 + K_{sv}[Q]$, where (I_0/I) is the ratio of fluorescence intensity in the absence and the presence of the quencher. K_{sv} and [Q] are the quenching constant and quencher concentration, respectively. A similar experiment with (ArBr)Ni@Bpy-sp^{2}c-COF at a different loading of ArBr yields $K_{sv} = 1.33 \times 10^5\ M^{-1}$. The 1.44×10^5 and 0.87×10^5 fold higher K_{sv}, respectively, further endorsed the enhance energy or transfer in an interlocked dual catalytic Ni@Bpy-sp^{2}c-COF compared to a discrete two-catalytic system.[7d,16] In multiple reports, the energy-excited Ni^{II} species was shown to be crucial in facilitating carbon–carbon and carbon–heteroatom bond-forming cross-coupling reactions *via* Ni–Br and Ni–Ar bond homolysis, C–O reductive elimination, and ligand–metal charge transfer.[17] We suspect that enhanced energy transfer in the interlocked Ni@Bpy-sp^{2}c-COF could facilitate diverse visible light-harvesting cross-coupling reactions.

With these favorable characteristics, we then evaluated the performance of the Ni@Bpy-sp^{2}c-COF in light-mediated cross-coupling reactions. We studied eight photoinduced C–X (X = B, C, N, O, P, S) bond-forming reactions to examine the scope and application of the Ni@Bpy-sp^{2}c-COF catalyst (Fig. 3).

First, the energy transfer-mediated cross-coupling of methyl 4-iodobenzoate **1** and Boc-Pro-OH **2** was studied. Pleasingly, we observed an outstanding catalytic efficiency of the Ni@Bpy-sp^{2}c-COF catalyst that offered 91% (83% isolated) yield of the desired C–O coupled product **3** at a low loading (0.90 mol% Ni) in the presence of organic base ^{t}BuNH^{i}Pr in DMF (0.5 M) under the irradiation of 65 W compact fluorescence light (CFL) (Fig. 3a; bar diagram, detailed in Tables S2 and S3†). Control experiments indicated that light, catalyst, base, and an inert atmosphere were necessary for this transformation. Notably, the reaction using Bpy-sp^{2}c-COF as a heterogeneous photosensitizer and (dtbbpy)$NiCl_2$ (0.9 mol%) as a homogeneous catalyst provides 48% of **3** under the same conditions, highlighting the

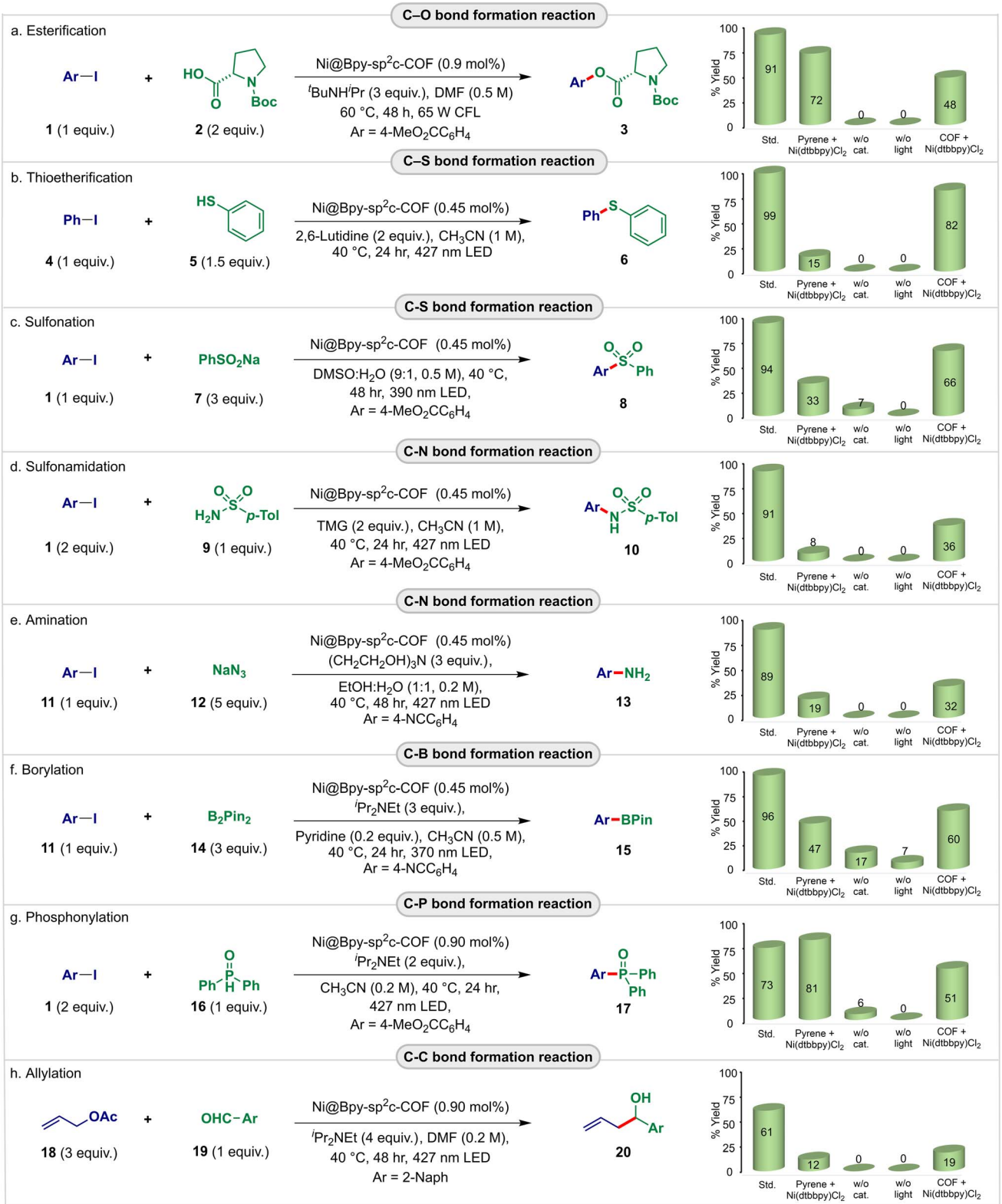

Fig. 3 Exploration of the Ni@Bpy-sp^{2}c-COF as the dual interlocked catalyst for the light-harvesting cross-coupling reactions (a–h). Reactions were performed at 0.1 mmol scales. Std conditions as defined in the equation. Homogeneous controls were performed with pyrene/(dtbbpy)$NiCl_2$ (5 mol%). Semi-heterogeneous controls were performed with Bpy-sp^{2}c-COF/(dtbbpy)$NiCl_2$ having the same loading as std conditions. See Tables S2–S17† for details.

beneficial effect of the interlocked catalyst system compared to the intermolecular semi-heterogeneous strategy. In comparison, 85% yield of **3** was obtained with homogeneous $Ir(ppy)_3$ (1 mol%) and (dtbbpy)$NiBr_2$ (5 mol%),[8a] whereas pyrene (5 mol%) and (dtbbpy)$NiCl_2$ (5 mol%) were necessary to obtain 72% yield of **3** under homogeneous conditions. This thus highlights that the Ni@Bpy-sp^{2}c-COF catalyst roughly suppresses the corresponding homogeneous catalysts by an order of magnitude.

We then studied the photocatalytic C–S coupling reaction. Pleasingly, Ni@Bpy-sp^{2}c-COF with 0.45 mol% Ni-loading efficiently catalyzed the coupling of iodobenzene **4** with thiophenol **5**, delivering diphenylthioether **6** in 99% yield (95% isolated) in the presence of 2,6-lutidine in CH_3CN (1 M) under the irradiation of a 427 nm blue light-emitting diode (LED) (Fig. 3b; bar diagram, detailed in Tables S4 and S5†). A similar comparison with the model reaction with homogeneous pyrene/(dtbbpy)$NiCl_2$ (5 mol%) that gave 15% of **6** again indicated that Ni@Bpy-sp^{2}c-COF outperformed its homogeneous counterparts by two orders of magnitude. This was further corroborated by a comparative time-dependent kinetic study (Fig. S16†).

A similar observation was made for the C–S coupling of methyl 4-iodobenzoate **1** with sodium benzenesulfinate **7** (Fig. 3c; bar diagram, detailed in Tables S6 and S7†). The Ni@Bpy-sp^{2}c-COF (0.45 mol% Ni-loading) catalyzed reaction produced methyl 4-(phenylsulfonyl)benzoate **8** in 94% yield, and the performance was several fold better than the homogeneous and semi-heterogeneous control.

With these successes, we were prompted to perform the redox-neutral C–N coupling reaction using **1** and *p*-toluenebenzenesulfonamide **9** as the coupling partners (Fig. 3d; bar diagram, detailed in Tables S8 and S9†). Pleasingly, the Ni@Bpy-sp^{2}c-COF (0.45 mol% Ni-loading) catalyzed photo–sulfonamidation reaction provided 91% yield of the C–N coupled product **10**. We also attempted the reductive aromatic amination reaction with sodium azide **12** as the nitrogen source for synthesizing high-value aniline derivatives (Fig. 3e; bar diagram, detailed in Tables S10 and S11†). Gratifyingly, our interlocked dual-catalyst Ni@Bpy-sp^{2}c-COF (0.45 mol% Ni-loading) efficiently catalyzed the reaction sacrificing triethanolamine as the electron donor in EtOH–H_2O (1 : 1, 0.2 M) under the irradiation of a 427 nm blue LED and the corresponding aniline **13** was obtained in 93% yield. Notably, the semiheterogeneous reaction using (dtbbpy)$NiCl_2$ and Bpy-sp^{2}c-COF as catalysts resulted in 36% and 32% yields of **10** and **13**, respectively, again highlighting the beneficial photoredox communication in the two-in-one catalyst system over the two distinct ones. Moreover, again in both cases, the Ni@Bpy-sp^{2}c-COF showed more than 40-fold superior activity than the homogeneous reaction with the pyrene/(dtbbpy)$NiCl_2$ (5 mol%) catalyst.

The catalytic versatility of the Ni@Bpy-sp^{2}c-COF could be expanded to the C–B bond formation reaction (Fig. 3f; bar diagram, detailed in Tables S12 and S13†). Organoboron compounds are resourceful intermediates with diverse applications.[18] Gratifyingly, with only 0.45 mol% Ni-loading, the Ni@Bpy-sp^{2}c-COF catalyst catalyzed the visible-light-induced borylation of 4-iodobenzonitrile **11** with bis(pinacolato)diboron **14** in CH_3CN (0.5 M) under the irradiation of a 370 nm LED. The product methyl 4-(4,4,5,5-tetramethyl-1,3,2-dioxaborolan-2-yl) benzoate **15** was obtained in 96% yield. The control experiments suggested the necessity of each reaction component for the success of the catalysis. More importantly, a 20-fold superior performance of the interlocked catalyst Ni@Bpy-sp^{2}c-COF over the homogenous reaction is noticed.

We then performed a C–P cross-coupling reaction to explore further the utility of the nickel-grafted sp^{2}c-COF in light-harvesting cross-coupling reactions. Considering the utility of the aryl phosphonates in medicinal chemistry and materials science,[19] we attempted a visible-light mediated phosphonylation reaction (Fig. 3g; bar diagram, detailed in Tables S14 and S15†). The Ni@Bpy-sp^{2}c-COF (0.90 mol% Ni-loading) catalyzed reaction of **1** with diphenylphosphine oxide **16** in the presence of ^{i}Pr$_2$NEt delivered methyl 4-(diphenylphosphoryl)benzoate **17** in 73% yield in CH_3CN (0.2 M) under 427 nm blue LED irradiation.

Finally, the Ni@Bpy-sp^{2}c-COF was applied for the Nozaki–Hiyama–Kishi-type cross-electrophile coupling between allyl acetate **18** and 2-naphthaldehyde **19** (Fig. 3h; bar diagram, detailed in Tables S16 and S17†).[13g] With ^{i}Pr$_2$NEt as the organic sacrificial reductant, the reductive C–C coupled product **20** was obtained in 61% yield in DMF (0.2 M) under 427 nm blue LED irradiation. Again, the control experiments illustrated the essential cooperation between the COF backbone and Ni-center in boosting the C–P and C–C bond-forming reactions. Although aryl chlorides performed poorly, aryl bromides smoothly participated in Ni@Bpy-sp^{2}c-COF-catalyzed diverse cross-coupling reactions as described in Fig. 3. The products were obtained in 32–84% yields (Tables S3–S15†).

Afterward, we explored the applicability and functional group compatibility for the Ni@Bpy-sp^{2}c-COF-catalyzed light-harvesting cross-coupling reactions. We modeled C–O and C–S coupling reactions for this purpose (Fig. 4 and 5). With the optimized conditions to hand, first, we tested different aliphatic cyclic carboxylic acids (Fig. 4). The reactions delivered moderate to good yields (42–80%) of the desired esters **21–24**. Notably, cyclopropyl (**23**) and adamantyl (**24**) groups were retained under these conditions. The activated internal (**25**) and terminal (**26**) olefins were also found to be compatible. Additionally, 3-phenylpropanoic acid (**27**), tetrahydro-2*H*-pyran-4-carboxylic acid (**28**), phenoxyacetic acid (**29**), and valproic acid (**30**) also steadily participated, delivering the C–O couple products in 49–78% yields.

The reaction was also compatible with a range of aryl carboxylic acids having electronically biased functional groups (electron neutral, rich, and poor) at the *ortho*-, *meta*-, and *para*-position of the aryl ring. The corresponding esters **31–39** were isolated in high 45–76% yields. Furthermore, a free thiol group was retained under the reaction conditions and gave a moderate 53% yield of the desired ester **40**. This also highlighted the selective coupling between two coupling partners. Notably, the heteroaryl ring of thiophene-2-carboxylic acid is also well suited to this strategy, and heteroaryl carboxylate ester **41** was isolated in 70% yield.

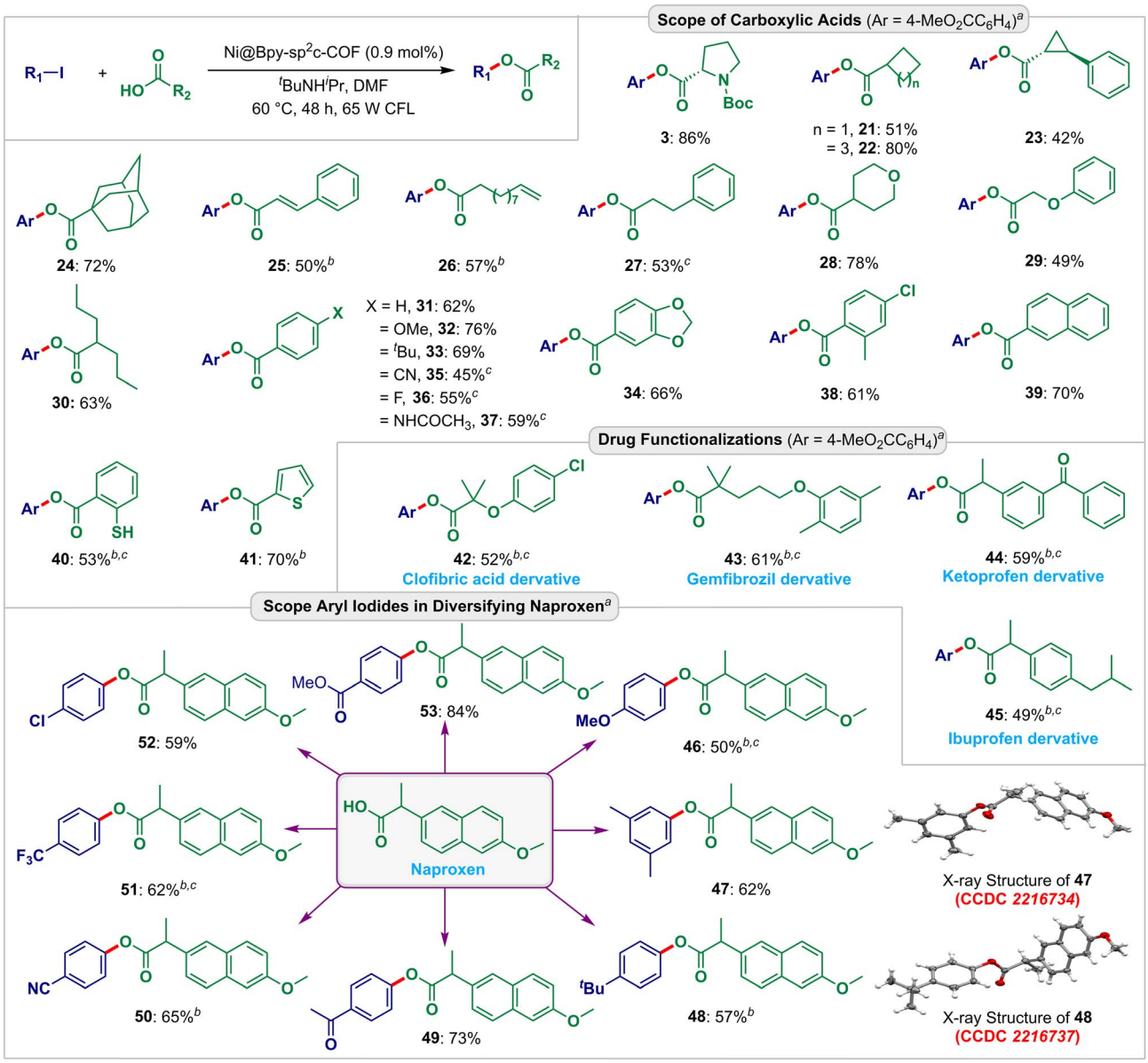

Fig. 4 Scopes and functional group compatibility for the Ni@Bpy-sp^{2}c-COF-catalyzed C–O coupling reactions. Isolated yield. The CCDC numbers (red color) are given in parenthesis for the X-ray crystal structure of **47** and **48** (ref. 20). [a]Reaction conditions: ArI (0.10 mmol), RCO_2H (0.2 mmol), Ni@Bpy-sp^{2}c-COF (2 mg, 0.9 mol% Ni), ^{t}BuNH^{i}Pr (0.3 mmol), DMF (0.2 mL) under 65 W CFL light irradiation at 40 °C for 48 h. [b]72 h. [c]Ni@Bpy-sp^{2}c-COF (3 mg, 1.35 mol% Ni).

To further exemplify the synthetic utility, we explored the esterification of drug molecules. The hypolipidemic drugs gemfibrozil (**42**) and clofibric acid (**43**), and the analgesics ketoprofen (**44**) and ibuprofen (**45**) could be esterified in good yields under these conditions.

The success of this protocol also prompted us to extend the scope for derivatizing the anti-inflammatory drug naproxen. Notably, both electron-rich and electron-poor aryl electrophiles could be utilized as the coupling partner yielding aryl naproxen esters **46–53** in 50–84% yields. The structures of **47** and **48** were confirmed by X-ray crystallography data analysis (CCDC no. 2216734 and 2216737, detailed in Fig. S19, S20, Tables S18 and S19†).[20]

Further scope and functional group compatibility were investigated for the visible-light-driven C–S bond coupling reaction (Fig. 5). We were elated to find that the interlocked dual catalyst enabled the coupling of a large variety of aryl and alkyl thiols with high efficiencies. Aryl thiols with a wide range of electronically biased substituents at different positions of the aryl ring underwent smooth C–S coupling reactions yielding the thioethers **54–59** in 70–86% yields. The photo-driven reaction also proceeded steadily with β-thionaphthol (**60**) and benzothiazole-2-thiol (**61**) giving the products in 78% and 49% yields, respectively. We then investigated the scope of aliphatic thiols. Diverse aliphatic thiols such as cyclohexanethiol (**62**), adamantanethiol (**63**), benzylthiol (**64**, **65**), and 2-

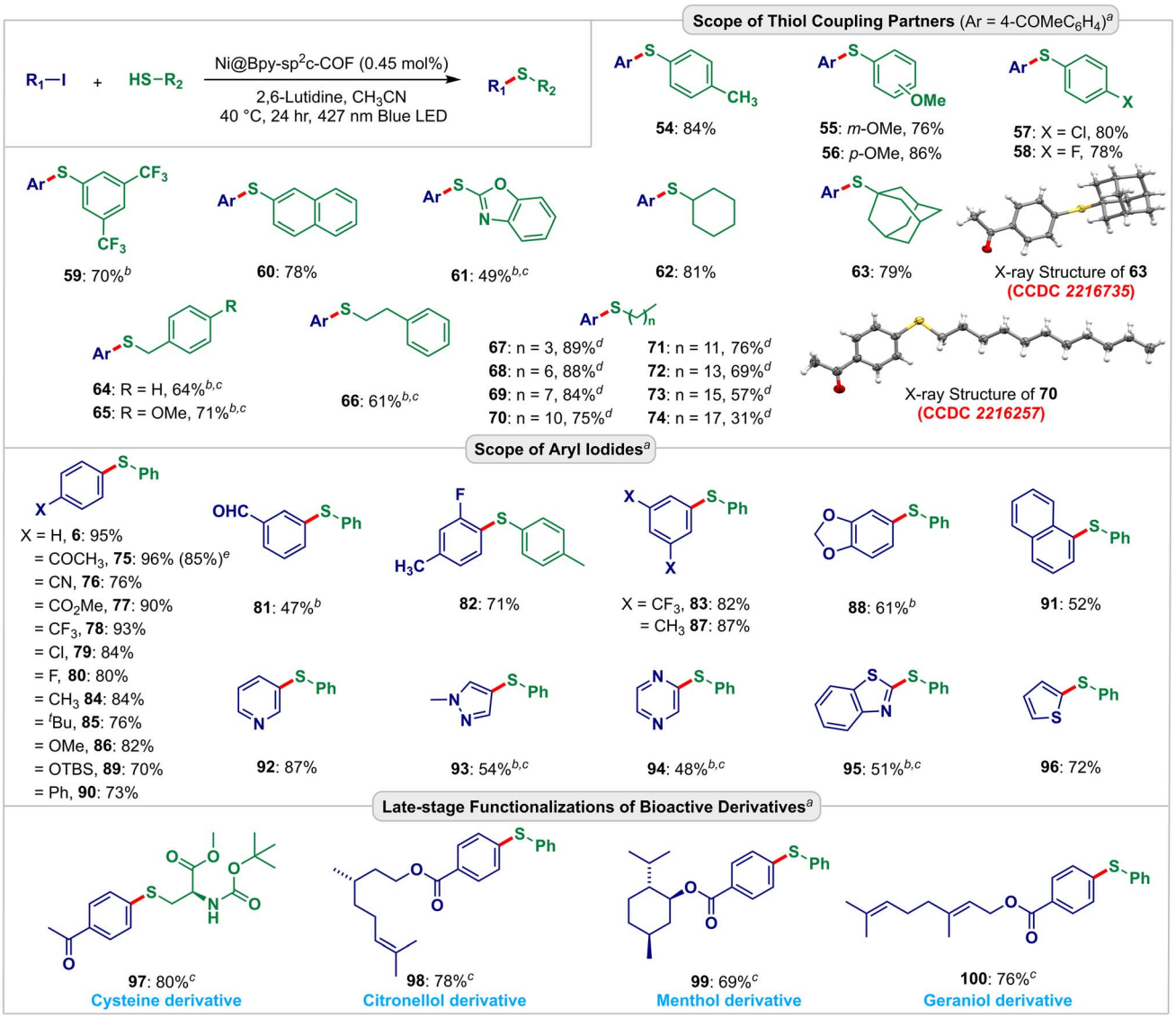

Fig. 5 Scopes and functional group compatibility for the Ni@Bpy-sp^{2}c-COF-catalyzed C–S coupling reactions. Isolated yield. The CCDC numbers (red color) are given in parentheses for the X-ray crystal structure of **63** and **70** (ref. 21). [a]Reaction conditions: aryl iodide (0.10 mmol), thiol (0.15 mmol), Ni@Bpy-sp^{2}c-COF (1 mg), 2,6-lutidine (0.2 mmol), CH_3CN (0.1 mL) under the irradiation of a 427 nm blue LED at 40 °C for 24 h. [b]Ni@Bpy-sp^{2}c-COF (0.95 mol% Ni), [c]48 h. [d]Thiol (0.3 mmol), [e]5 mmol scale.

phenylethanethiol (**66**) were employed and delivered the desired products in 61–81% yields. We also used different long-chain aliphatic thiols (**67–74**) to analyze the size selectivity. As anticipated, the experiment showed that with the increase in chain length, the yields of the corresponding thioether product gradually decreased. The X-ray crystallography further confirmed the structures of **63** and **70** (CCDC no. 2216735 and 2216257, detailed in Fig. S21, S22, Tables S20 and S21†).[21]

The Ni@Bpy-sp^{2}c-COF-catalyzed C–S coupling reaction also accommodated a wide range of electron-poor **75–83** and electron-rich **84–88** aryl coupling partners to produce the thioethers in 47–96% yield. A broad range of synthetically useful functional groups like acetyl (**75**), nitrile (**76**), ester (**77**), trifluoromethyl (**78**, **83**), chloride (**79**), fluoride (**80**, **82**), formyl (**81**), ether (**86**), dioxole (**88**), and silyl ether (**89**) were compatible under these light-harvesting conditions. Biphenyl (**90**), naphthalene (**91**), and, more importantly, different heterocycles, including pyridine (**92**), pyrazole (**93**), pyrazine (**94**), benzothiazole (**95**), and thiophene (**96**) compounds smoothly took part in this cross-coupling reaction and produced the corresponding thioethers in 48–87% yield. Furthermore, the synthetic application of the developed strategy was demonstrated in diversifying derivatives of amino acid, cystine (**97**), and monoterpenoids such as citronellol (**98**), menthol (**99**), and geraniol (**100**) that gave the corresponding products 69–80% yield. A gram scale visible-light-driven C–S cross-coupling of 4-iodoacetophenone and 4-methoxythiophenol was also performed, and it delivered 1.10 g (85% yield) of **75** (detailed in Fig. S23†).

The plausible mechanistic cycles for the Ni@Bpy-sp^{2}c-COF-catalyzed cross-coupling reactions are depicted in Section S-

XII.† We believe that the C–O, C–N (with sulfonamide), and C–B coupling reactions proceed *via* energy transfer pathways. In comparison, the C–S, C–N (with azide), C–P, and C–C coupling reactions proceeded *via* electron-transfer routes. As a representative, the mechanisms of C–S, and C–O cross-coupling reactions were investigated by quenching studies and control experiments. We observed that thiophenol **5** quenches the luminescence of the excited Ni@Bpy-sp^{2}c-COF at a very high rate $K_{sv} = 10.1\ M^{-1}$, and the quenching rate was almost 5 times higher than that for iodobenzene **4** (Fig. S17a†). This suggested a SET mechanism and the existence of radicals. The reaction in the presence of a well-known radical trapping agent 2,2,6,6-tetramethylpiperidine 1-oxyl (TEMPO) gave a low 9% yield of **6**. Besides, we could isolate and characterize the TEMPO-trapped intermediate *via* HRMS and ^{1}H NMR (Fig. S17b†). These experiments strongly support a SET mechanism for the thioetherification reaction proposed in Fig. S32, Section S-XII.† In comparison, for the C–O coupling reaction, we observed similar Stern–Volmer quenching rates for ^{t}BuNH^{i}Pr and ^{t}BuNH^{i}Pr in the presence of cyclobutanecarboxylic acid (Fig. S18†). Besides, the reaction was not significantly affected by the presence of TEMPO. These results point toward an energy transfer rather than a SET pathway (Fig. S31, Section S-XII†).[8a,22] Overall, we stress that the pyrene-based sp^2 carbon-conjugated Bpy-sp^{2}c-COF anchored nickel catalysts performed all these reactions with very high efficiencies.

Finally, the intriguing characteristics of this heterogeneous catalyst were further corroborated by its recovery and reusability. The Ni@Bpy-sp^{2}c-COF catalyst was filtered after the coupling between **4** and **5** and reused for the next catalytic cycle. We observed 86% yield after the 6th cycle, indicating the catalyst's chemical stability and excellent reusability (Fig. S24†). Only 0.21 wt% leaching of Ni was observed after the 6th cycle. The recovered Ni@Bpy-sp^{2}c-COF catalyst after the 1st cycle was further characterized by TEM, SEM, IR, and XPS to display the robustness of the catalyst. The TEM and SEM images indicated that the nickel-black nanoparticle formation did not happen during catalysis (Fig. S25 and S27†). In addition, the micro rods and cluster shapes of the Ni@Bpy-sp^{2}c-COF catalyst were unaltered with a homogeneous distribution of nickel (Fig. S26 and S28†). The IR and XPS analysis also revealed the consistency of the chemical identity for the recycled Ni-loaded COF. The IR spectrum of the recovered catalyst material indicated no apparent change near 2216 cm^{-1} (C≡N) (Fig. S29†). The XPS spectrum of the recycled material for Ni ($2p_{3/2}$) and Ni ($2p_{1/2}$) peaks (at 856.8 eV and 874.4 eV, respectively) also remained unchanged after catalysis (Fig. S30†). Accumulation of these results confirmed that the properties and morphology of the catalyst material were retained even after reactions.

Conclusions

In summary, we post-synthetically engineered an sp^2 carbon-conjugated COF with a transition metal for visible light-mediated C–X cross-coupling reactions. The C=C linked COF was synthesized *via* the Knoevenagel condensation reaction and decorated with nickel *via* bipyridine units. The interlocking of the light-harvesting COF backbone and the redox-active Ni-units in the COF pores facilitates the dual catalysis mediated by light and the transition metal and enables different C–X (X = B, C, N, O, P, S) cross-coupling reactions with efficiency orders of magnitude higher than its homogeneous counterpart. Photoluminescence, cyclic voltammetry, kinetic, and control experiments corroborated the higher efficiency of this two-in-one catalyst system. The bipyridine-anchored catalyst prevented metal leaching and nickel-black formation, enabling selective coupling without compromising performance and reusability. The catalyst tolerated a diverse range of coupling partners having various steric and electronic properties and showed excellent functional group tolerance for the model reactions. The reactions could also be performed on a gram scale and utilized to diversify complex molecules. The work demonstrates a strategy of mono-metalation in COFs to create a platform for metallaphotoredox dual catalysis, highlighting its undiscovered potential in sustainable light-harvesting chemical synthesis.

Data availability

The ESI† includes all experimental details, including optimization of the synthetic method, synthesis and characterization of all materials and products reported in this study, and mechanistic studies. NMR spectra of all products, and crystallography, details are included as well.

Author contributions

A. J. and B. M. conceived and designed the project. A. J., S. D., S. K., and K. K. performed experiments. S. D., S. K., and K. K. contributed equally to this work. A. J. and B. M. wrote the manuscript. B. M. acquired the funding and directed the research.

Conflicts of interest

There are no conflicts to declare.

Acknowledgements

A. J. acknowledges CSIR for the PhD fellowship. S. D., S. K., and K. K. thank IISER Kolkata for their support. B. M. acknowledges DST SERB, GOI (grant no. CRG/2019/001232) for financial support. We sincerely thank Prof. Rahul Banerjee (IISER K) for his help in material characterization and discussion.

References

1 (*a*) A. P. Cote, A. I. Benin, N. W. Ockwig, M. O'Keeffe, A. J. Matzger and O. M. Yaghi, *Science*, 2005, **310**, 1166–1170; (*b*) C. S. Diercks and O. M. Yaghi, *Science*, 2017, **355**, eaal1585; (*c*) J. Jiang, Y. Zhao and O. M. Yaghi, *J. Am. Chem. Soc.*, 2016, **138**, 3255–3265; (*d*) J. H. Kim, D. W. Kang, H. Yun, M. Kang, N. Singh, J. S. Kim and C. S. Hong, *Chem. Soc. Rev.*, 2022, **51**, 43–56; (*e*) R. K. Sharma, P. Yadav, M. Yadav, R. Gupta, P. Rana,

A. Srivastava, R. Zbořil, R. S. Varma, M. Antonietti and M. B. Gawande, *Mater. Horiz.*, 2020, **7**, 411–454; (*f*) J. Francis Kurisingal, H. Kim, J. Hyeak Choe and C. Seop Hong, *Coord. Chem. Rev.*, 2022, **473**, 214835; (*g*) E. Jin, J. Li, K. Geng, Q. Jiang, H. Xu, Q. Xu and D. Jiang, *Nat. Commun.*, 2018, **9**, 4143; (*h*) A. M. Evans, A. Giri, V. K. Sangwan, S. Xun, M. Bartnof, C. G. Torres-Castanedo, H. B. Balch, M. S. Rahn, N. P. Bradshaw, E. Vitaku, D. W. Burke, H. Li, M. J. Bedzyk, F. Wang, J.-L. Brédas, J. A. Malen, A. J. H. McGaughey, M. C. Hersam, W. R. Dichtel and P. E. Hopkins, *Nat. Mater.*, 2021, **20**, 1142–1148; (*i*) B. Garai, D. Shetty, T. Skorjanc, F. Gándara, N. Naleem, S. Varghese, S. K. Sharma, M. Baias, R. Jagannathan, M. A. Olson, S. Kirmizialtin and A. Trabolsi, *J. Am. Chem. Soc.*, 2021, **143**, 3407–3415.

2 (*a*) H. Lyu, C. S. Diercks, C. Zhu and O. M. Yaghi, *J. Am. Chem. Soc.*, 2019, **141**, 6848–6852; (*b*) H. Xu, J. Gao and D. Jiang, *Nat. Chem.*, 2015, **7**, 905–912; (*c*) Q. Sun, B. Aguila, J. Perman, N. Nguyen and S. Ma, *J. Am. Chem. Soc.*, 2016, **138**, 15790–15796; (*d*) H. S. Sasmal, S. Bag, B. Chandra, P. Majumder, H. Kuiry, S. Karak, S. Sen Gupta and R. Banerjee, *J. Am. Chem. Soc.*, 2021, **143**, 8426–8436; (*e*) M. d. J. Velásquez-Hernández, E. Astria, S. Winkler, W. Liang, H. Wiltsche, A. Poddar, R. Shukla, G. Prestwich, J. Paderi, P. Salcedo-Abraira, H. Amenitsch, P. Horcajada, C. J. Doonan and P. Falcaro, *Chem. Sci.*, 2020, **11**, 10835–10843; (*f*) W. Liang, F. Carraro, M. B. Solomon, S. G. Bell, H. Amenitsch, C. J. Sumby, N. G. White, P. Falcaro and C. J. Doonan, *J. Am. Chem. Soc.*, 2019, **141**, 14298–14305; (*g*) D. A. Vazquez- Molina, G. M. Pope, A. A. Ezazi, J. L. Mendoza-Cortes, J. K. Harper and F. J. Uribe-Romo, *Chem. Commun.*, 2018, **54**, 6947–6950; (*h*) F. J. Uribe-Romo, C. J. Doonan, H. Furukawa, K. Oisaki and O. M. Yaghi, *J. Am. Chem. Soc.*, 2011, **133**, 11478–11481; (*i*) M. M. Sadiq, K. Konstas, P. Falcaro, A. J. Hill, K. Suzuki and M. R. Hill, *Cell Rep. Phy. Sci*, 2020, **1**, 100070.

3 (*a*) G.-B. Wang, S. Li, C.-X. Yan, F.-C. Zhu, Q.-Q. Lin, K.-H. Xie, Y. Geng and Y.-B. Dong, *J. Mater. Chem. A*, 2020, **8**, 6957–6983; (*b*) J. L. Segura, S. Royuela and M. Mar Ramos, *Chem. Soc. Rev.*, 2019, **48**, 3903–3945; (*c*) J.-Y. Zeng, X.-S. Wang and X.-Z. Zhang, *Chem. –Eur. J.*, 2020, **26**, 16568–16581; (*d*) S. Trenker, L. Grunenberg, T. Banerjee, G. Savasci, L. M. Poller, K. I. M. Muggli, F. Haase, C. Ochsenfeld and B. V. Lotsch, *Chem. Sci.*, 2021, **12**, 15143–15150; (*e*) T. Skorjanc, D. Shetty, M. E. Mahmoud, F. Gándara, J. I. Martinez, A. K. Mohammed, S. Boutros, A. Merhi, E. O. Shehayeb, C. A. Sharabati, P. Damacet, J. Raya, S. Gardonio, M. Hmadeh, B. R. Kaafarani and A. Trabolsi, *ACS Appl. Mater. Interfaces*, 2022, **14**, 2015–2022; (*f*) M. Bhadra, S. Kandambeth, M. K. Sahoo, M. Addicoat, E. Balaraman and R. Banerjee, *J. Am. Chem. Soc.*, 2019, **141**, 6152–6156.

4 (*a*) W. Zhong, R. Sa, L. Li, Y. He, L. Li, J. Bi, Z. Zhuang, Y. Yu and Z. Zou, *J. Am. Chem. Soc.*, 2019, **141**, 7615–7621; (*b*) Z. Fu, X. Wang, A. M. Gardner, X. Wang, S. Y. Chong, G. Neri, A. J. Cowan, L. Liu, X. Li, A. Vogel, R. Clowes, M. Bilton, L. Chen, R. S. Sprick and A. I. Cooper, *Chem. Sci.*, 2020, **11**, 543–550; (*c*) C. Wang, S. Cao and W.-F. Fu, *Chem. Commun.*, 2013, **49**, 11251–11253; (*d*) S. Yang, W. Hu, X. Zhang, P. He, B. Pattengale, C. Liu, M. Cendejas, I. Hermans, X. Zhang, J. Zhang and J. Huang, *J. Am. Chem. Soc.*, 2018, **140**, 14614–14618; (*e*) Z. He, J. Goulas, E. Parker, Y. Sun, X.-d. Zhou and L. Fei, *Catal. Today*, 2023, **409**, 103–118; (*f*) H. Wang, H. Wang, Z. Wang, L. Tang, G. Zeng, P. Xu, M. Chen, T. Xiong, C. Zhou, X. Li, D. Huang, Y. Zhu, Z. Wang and J. Tang, *Chem. Soc. Rev.*, 2020, **49**, 4135–4165.

5 (*a*) H.-S. Lu, W.-K. Han, X. Yan, C.-J. Chen, T. Niu and Z.-G. Gu, *Angew. Chem., Int. Ed.*, 2021, **60**, 17881–17886; (*b*) A. López-Magano, B. Ortín-Rubio, I. Imaz, D. Maspoch, J. Alemán and R. Mas-Ballesté, *ACS Catal.*, 2021, **11**, 12344–12354; (*c*) W. Dong, Y. Yang, Y. Xiang, S. Wang, P. Wang, J. Hu, L. Rao and H. Chen, *Green Chem.*, 2021, **23**, 5797–5805; (*d*) H. Chen, W. Liu, A. Laemont, C. Krishnaraj, X. Feng, F. Rohman, M. Meledina, Q. Zhang, R. Van Deun, K. Leus and P. Van Der Voort, *Angew. Chem., Int. Ed.*, 2021, **60**, 10820–10827.

6 (*a*) C. K. Prier, D. A. Rankic and D. W. C. MacMillan, *Chem. Rev.*, 2013, **113**, 5322–5363; (*b*) A. Y. Chan, I. B. Perry, N. B. Bissonnette, B. F. Buksh, G. A. Edwards, L. I. Frye, O. L. Garry, M. N. Lavagnino, B. X. Li, Y. Liang, E. Mao, A. Millet, J. V. Oakley, N. L. Reed, H. A. Sakai, C. P. Seath and D. W. C. MacMillan, *Chem. Rev.*, 2022, **122**, 1485–1542; (*c*) J. A. Terrett, J. D. Cuthbertson, V. W. Shurtleff and D. W. C. MacMillan, *Nature*, 2015, **524**, 330–334; (*d*) A. Tlili and S. Lakhdar, *Angew. Chem., Int. Ed.*, 2021, **60**, 19526–19549; (*e*) S. Morand, W. Lecroq, P. Jubault, S. Lakhdar, J.-P. Bouillon and S. Couve-Bonnaire, *Org. Lett.*, 2022, **24**, 8343–8347; (*f*) F. Rammal, D. Gao, S. Boujnah, A. C. Gaumont, A. A. Hussein and S. Lakhdar, *Org. Lett.*, 2020, **22**, 7671–7675; (*g*) P. Rai, K. Maji, S. K. Jana and B. Maji, *Chem. Sci.*, 2022, **13**, 12503–12510.

7 (*a*) M. S. Oderinde, N. H. Jones, A. Juneau, M. Frenette, B. Aquila, S. Tentarelli, D. W. Robbins and J. W. Johannes, *Angew. Chem., Int. Ed.*, 2016, **55**, 13219–13223; (*b*) B. Liu, C.-H. Lim and G. M. Miyake, *J. Am. Chem. Soc.*, 2017, **139**, 13616–13619; (*c*) E. B. Corcoran, M. T. Pirnot, S. Lin, S. D. Dreher, D. A. DiRocco, I. W. Davies, S. L. Buchwald and D. W. C. MacMillan, *Science*, 2016, **353**, 279–283; (*d*) K. Wang, H. Jiang, H. Liu, H. Chen and F. Zhang, *ACS Catal.*, 2022, **12**, 6068–6080; (*e*) M. Traxler, S. Gisbertz, P. Pachfule, J. Schmidt, J. Roeser, S. Reischauer, J. Rabeah, B. Pieber and A. Thomas, *Angew. Chem., Int. Ed.*, 2022, **61**, e202117738; (*f*) J. Li, C.-Y. Huang and C.-J. Li, *Chem*, 2022, **8**, 2419–2431; (*g*) N. Alandini, L. Buzzetti, G. Favi, T. Schulte, L. Candish, K. D. Collins and P. Melchiorre, *Angew. Chem., Int. Ed.*, 2020, **59**, 5248–5253.

8 (*a*) E. R. Welin, C. Le, D. M. Arias-Rotondo, J. K. McCusker and D. W. C. MacMillan, *Science*, 2017, **355**, 380–385; (*b*) A. Saha, S. Guin, W. Ali, T. Bhattacharya, S. Sasmal, N. Goswami, G. Prakash, S. K. Sinha, H. B. Chandrashekar, S. Panda, S. S. Anjana and D. Maiti, *J. Am. Chem. Soc.*, 2022, **144**, 1929–1940; (*c*) M. S. Oderinde, N. H. Jones, A. Juneau, M. Frenette, B. Aquila, S. Tentarelli, D. W. Robbins and J. W. Johannes, *Angew. Chem., Int. Ed.*,

2016, **55**, 13219–13223; (*d*) R. Ruzi, K. Liu, C. Zhu and J. Xie, *Nat. Commun.*, 2020, **11**, 3312; (*e*) C.-H. Lim, M. Kudisch, B. Liu and G. M. Miyake, *J. Am. Chem. Soc.*, 2018, **140**, 7667–7673.

9 (*a*) I. Ghosh, J. Khamrai, A. Savateev, N. Shlapakov, M. Antonietti and B. König, *Science*, 2019, **365**, 360–366; (*b*) S. Gisbertz, S. Reischauer and B. Pieber, *Nat. Catal.*, 2020, **3**, 611–620; (*c*) B. Pieber, J. A. Malik, C. Cavedon, S. Gisbertz, A. Savateev, D. Cruz, T. Heil, G. Zhang and P. H. Seeberger, *Angew. Chem. Int. Ed.*, 2019, **58**, 9575–9580; (*d*) Y. Pan, N. Zhang, C.-H. Liu, S. Fan, S. Guo, Z.-M. Zhang and Y.-Y. Zhu, *ACS Catal.*, 2020, **10**, 11758–11767; (*e*) S. Das, K. Murugesan, G. J. Villegas Rodríguez, J. Kaur, J. P. Barham, A. Savateev, M. Antonietti and B. König, *ACS Catal.*, 2021, **11**, 1593–1603.

10 (*a*) Y.-Y. Zhu, G. Lan, Y. Fan, S. S. Veroneau, Y. Song, D. Micheroni and W. Lin, *Angew. Chem., Int. Ed.*, 2018, **57**, 14090–14094; (*b*) G. Lan, Y. Quan, M. Wang, G. T. Nash, E. You, Y. Song, S. S. Veroneau, X. Jiang and W. Lin, *J. Am. Chem. Soc.*, 2019, **141**, 15767–15772; (*c*) H. Zhang, Z. Lin, P. Kidkhunthod and J. Guo, *Angew. Chem., Int. Ed.*, 2023, **62**, e202217527.

11 A. Jati, K. Dey, M. Nurhuda, M. A. Addicoat, R. Banerjee and B. Maji, *J. Am. Chem. Soc.*, 2022, **144**, 7822–7833.

12 (*a*) R. Bu, L. Zhang, X.-Y. Liu, S.-L. Yang, G. Li and E.-Q. Gao, *ACS Appl. Mater. Interfaces*, 2021, **13**, 26431–26440; (*b*) Y. Xiang, W. Dong, P. Wang, S. Wang, X. Ding, F. Ichihara, Z. Wang, Y. Wada, S. Jin, Y. Weng, H. Chen and J. Ye, *Appl. Catal., B*, 2020, **274**, 119096; (*c*) K. Geng, T. He, R. Liu, S. Dalapati, K. T. Tan, Z. Li, S. Tao, Y. Gong, Q. Jiang and D. Jiang, *Chem. Rev.*, 2020, **120**, 8814–8933.

13 (*a*) M. S. Oderinde, M. Frenette, D. W. Robbins, B. Aquila and J. W. Johannes, *J. Am. Chem. Soc.*, 2016, **138**, 1760–1763; (*b*) M. J. Cabrera-Afonso, Z.-P. Lu, C. B. Kelly, S. B. Lang, R. Dykstra, O. Gutierrez and G. A. Molander, *Chem. Sci.*, 2018, **9**, 3186–3191; (*c*) T. Kim, S. J. McCarver, C. Lee and D. W. C. MacMillan, *Angew. Chem., Int. Ed.*, 2018, **57**, 3488–3492; (*d*) A. Vijeta, C. Casadevall and E. Reisner, *Angew. Chem., Int. Ed.*, 2022, **61**, e202203176; (*e*) D. Lai, S. Ghosh and A. Hajra, *Org. Biomol. Chem.*, 2021, **19**, 4397–4428; (*f*) J. Xuan, T.-T. Zeng, J.-R. Chen, L.-Q. Lu and W.-J. Xiao, *Chem. –Eur. J.*, 2015, **21**, 4962–4965; (*g*) A. Gualandi, G. Rodeghiero, A. Faraone, F. Patuzzo, M. Marchini, F. Calogero, R. Perciaccante, T. P. Jansen, P. Ceroni and P. G. Cozzi, *Chem. Commun.*, 2019, **55**, 6838–6841.

14 A comparison of the state-of-the-art photocatalytic cross-coupling reactions and this work is included in Section S-XIII of the ESI†

15 D.-L. Zhu, R. Xu, Q. Wu, H.-Y. Li, J.-P. Lang and H.-X. Li, *J. Org. Chem.*, 2020, **85**, 9201–9212.

16 Y. Fan, D. W. Kang, S. Labalme, J. Li and W. Lin, *Angew. Chem., Int. Ed.*, 2023, **62**, e202218908.

17 (*a*) D. R. Heitz, J. C. Tellis and G. A. Molander, *J. Am. Chem. Soc.*, 2016, **138**, 12715–12718; (*b*) E. R. Welin, C. Le, D. M. Arias-Rotondo, J. K. McCusker and D. W. C. MacMillan, *Science*, 2017, **355**, 380–385; (*c*) M. Kudisch, C.-H. Lim, P. Thordarson and G. M. Miyake, *J. Am. Chem. Soc.*, 2019, **141**, 19479–19486; (*d*) S. I. Ting, S. Garakyaraghi, C. M. Taliaferro, B. J. Shields, G. D. Scholes, F. N. Castellano and A. G. Doyle, *J. Am. Chem. Soc.*, 2020, **142**, 5800–5810.

18 (*a*) N. A. Petasis, *Aust. J. Chem.*, 2007, **60**, 795–798; (*b*) C. A. McClary and M. S. Taylor, *Carbohydr. Res.*, 2013, **381**, 112–122.

19 T. Baumgartner and R. Réau, *Chem. Rev.*, 2006, **106**, 4681–4727.

20 Detailed crystallographic data information for CCDC 2216734 (compound **47**) and CCDC 2216737 (compound **48**) is presented in the ESI (Fig. S19, S20, Tables S18 and S19†).

21 Detailed crystallographic data information for CCDC 2216735 (compound **63**) and CCDC 2216257 (compound **70**) is presented in the ESI (Fig. S21, S22, Tables S20 and S21†).

22 D.-L. Zhu, H.-X. Li, Z.-M. Xu, H.-Y. Li, D. J. Young and J.-P. Lang, *Org. Chem. Front.*, 2019, **6**, 2353–2359.